HHS Public Access

Author manuscript

Nat Med. Author manuscript; available in PMC 2016 November 01.

Published in final edited form as:

Nat Med. 2016 May ; 22(5): 488–496. doi:10.1038/nm.4070.

ROR-γ drives androgen receptor expression and represents a therapeutic target in castration-resistant prostate cancer

Junjian Wang[1], **June X. Zou**[1], **Xiaoqian Xue**[2], **Demin Cai**[1], **Yan Zhang**[2], **Zhijian Duan**[1], **Qiuping Xiang**[2], **Joy C. Yang**[3], **Maggie C. Louie**[4], **Alexander D. Borowsky**[5], **Allen C. Gao**[3,8], **Christopher P. Evans**[3,8], **Kit S. Lam**[1,8], **Jianzhen Xu**[6], **Hsing-Jien Kung**[1,8], **Ronald M. Evans**[7], **Yong Xu**[2], and **Hong-Wu Chen**[1,8]

[1]Department of Biochemistry and Molecular Medicine, School of Medicine, University of California, Davis, California, USA

[2]Institute of Chemical Biology, Guangzhou Institutes of Biomedicine and Health, Chinese Academy of Sciences, No. 190 Kaiyuan Avenue, Guangzhou, China

[3]Department of Urology, School of Medicine, University of California, Davis, California, USA

[4]Department of Natural Sciences and Mathematics, Dominican University of California, San Rafael, California, USA

[5]Department of Pathology and Laboratory Medicine, School of Medicine, University of California, Davis, California, USA

[6]Shantou University Medical College, No. 22 Xinling Road, Shantou, China

[7]Gene Expression Laboratory, Salk Institute, Howard Hughes Medical Institute, Salk Institute, La Jolla, California, USA

[8]Comprehensive Cancer Center, School of Medicine, University of California, Davis, Sacramento, California, USA

Abstract

The androgen receptor (AR) is overexpressed and hyperactivated in human castration-resistant prostate cancer (CRPC). However, the determinants of AR overexpression in CRPC are poorly defined. Here we show that retinoid acid receptor-related orphan receptor γ (ROR-γ) is overexpressed and amplified in metastatic CRPC tumors, and that ROR-γ drives AR expression in the tumors. ROR-γ recruits coactivators SRC-1 and -3 to an AR-RORE to stimulate AR gene

Correspondence should be addressed to H-W.C. (hwzchen@ucdavis.edu) or Y.X. (xu_yong@gibh.ac.cn).

Accession codes. Gene Expression Omnibus: RNA-seq data are available under accession code GSE72483. ChIP-seq data are available under accession code GSE72714.

AUTHOR CONTRIBUTIONS

H-W.C., J.W. and J.X.Z. conceived and initiated the research. H-W.C., J.W., Y.X., R.M.E., and H-J.K. designed the research. J.W., J.X.Z., X.X., D.C., Y.Z., Z.D., Q.X., J.C.Y. and M.C.L. performed the experiments. H-W.C., J.W., J.X.Z., J. X. Y.X. M.C.L. and A.D.B. analyzed the data. H-W.C. J.W., Y.X., A.C.G., C.P.E., K.S.L., H.J.K. and R.M.E. wrote and/or edited the manuscript.

COMPETING FINANCIAL INTERESTS

The authors declare no competing financial interests.

transcription. ROR-γ antagonists suppress the expression of AR and its variant AR-V7 in prostate cancer (PCa) cell lines and tumors. ROR-γ antagonists also markedly diminish genome-wide AR binding, H3K27ac abundance and expression of the AR gene network. Lastly, ROR-γ antagonists suppressed tumor growth in multiple AR-expressing but not AR-negative xenograft PCa models, and effectively sensitized CRPC tumors to enzalutamide, without overt toxicity in mice. Together, these results establish ROR-γ as a key player in CRPC by acting upstream of AR and a potential therapeutic target for advanced PCa.

Persistent or reactivated signaling by androgen receptor (AR), a member of the nuclear receptor (NR) superfamily, drives progression of prostate cancer to a deadly form of the disease, namely metastatic castration-resistant prostate cancer (mCRPC). Tumors in most mCRPC patients express abundant AR, regardless of whether the gene encoding AR is amplified or mutated[1]. Recently approved therapeutics such as androgen signaling inhibitor enzalutamide (ENZ) and androgen synthesis inhibitor abiraterone (ABI) benefit some patients. However, *de novo* and acquired resistance appears inevitable. In addition to high expression of the full-length AR and high intratumoral androgen synthesis, tumor cell expression of alternatively spliced variants of AR such as AR-V7 that lack a functional ligand binding domain (LBD) constitutes another major resistance mechanism[2,3]. Current therapeutics development is still largely focused on anti-androgens with increased potencies, although agents that can disrupt AR N-terminal domain functionality or promote AR protein degradation are also being investigated[4–9]. However, little is known about which factor(s) drives AR gene expression in the mCRPC context.

The RAR-related orphan receptors (RORs) ROR-α, -β and -γ (with gene name *RORA, RORB* and *RORC* respectively) are NRs with distinct tissue expression patterns and likely play different physiological functions[10,11]. T cells express an isoform, ROR-γt encoded by RORC2, which differs from ROR-γ in the N-terminus due to T cell-specific promoter usage. ROR-γt is essential for differentiation of T cells that produce interleukin 17 (IL-17). Aboundant IL-17 promotes autoimmune diseases. As such, multiple ROR-γ antagonists and inverse agonists are being developed for therapeutic purposes[10,12]. Like other RORs, ROR-γ binds to specific ROR response elements (ROREs) at its genomic targets likely as monomer and can display a constitutive transactivation function in the absence of ligand[13,14]. ROR-γ-deficient mice are relatively healthy and fertile[15]. However, the expression and function of ROR-γ in human tumor cells remain largely unexplored.

In this study, we found that ROR-γ is highly overexpressed in tumors from mCRPC patients. ROR-γ functions as a key determinant of AR overexpression and aberrant signaling in mCRPC tumors. ROR-γ-selective antagonists inhibit AR gene expression, AR genome-wide binding, and growth of mCRPC cell lines in vitro and in mouse xenografts. Thus, our findings establish ROR-γ as a previously unsuspected key player and a novel therapeutic target for mCRPC.

RESULTS

ROR-γ expression and function in metastatic CRPC

Because NRs are attractive therapeutic targets[16,17], we reasoned that identification of NRs other than AR that play a crucial role in prostate cancer progression may lead to development of therapeutics for CRPC. We thus queried gene expression datasets from human benign, primary prostate cancer and metastatic prostate cancer samples and searched for NRs with altered expression in metastatic compared to benign and primary tumor tissue. In both datasets, the expression of ROR-α and ROR-β was significantly lower in metastatic tumors when compared to benign prostate tissue or localized tumors; in contrast, the expression of ROR-γ was significantly higher in metastatic tumors (Fig. 1a and Supplementary Fig. 1a). In addition, the ROR-γ gene *RORC* was amplified in 6% of metastic CRPC tumors in a recent study[18] (Supplementary Fig. 1a). Immunohistochemistry analysis of benign prostate and prostate tumors revealed that nuclear ROR-γ is overexpressed in over 50% of the tumors, and high levels of ROR-γ protein are significantly associated with tumor metastasis (Fig. 1b and Supplementary Fig. 1b). ROR-γ protein was readily detected by immunoblot in AR-positive cancer cell lines derived from CRPC tumors (e.g. LNCaP, C4-2B, 22Rv1, VCaP, PC346C and LAPC4), but not in the non-malignant human prostate epithelial cells (RWPE1 and PNT-2) (Fig. 1c).

Next, we examined the function of ROR-γ in prostate cancer. Knockdown of ROR-γ by different *RORC* siRNAs markedly inhibited the growth of LNCaP and its CRPC derivative C4-2B cells (Fig. 1d and Supplementary Fig. 1c). The strong growth inhibition was also observed in other androgen-sensitive and CRPC models such as VCaP and 22Rv1, but not in AR-negative PC-3 cells. ROR-γ knockdown also resulted in induction of apoptosis, as demonstrated by the activation of caspase3/7 and cleavage of PARP1, and suppression of proteins relevant to oncogenesis, proliferation and survival (e.g. cyclin-A, -E, -D3, Cdc2, Cdc6, and Bcl-xL, Myc and ERG (Fig. 1e, f; Supplementary Fig. 1d). Consistent with its crucial role in proliferation and survival, ectopic expression of ROR-γ in androgen-sensitive LNCaP cells promoted their growth in androgen-deprived conditions (Supplementary Fig. 1e).

ROR-γ-selective antagonists inhibit CRPC growth and survival

Recent studies identified several ROR-γ-specific antagonists (e.g. SR2211, GSK805, XY011/8k; Fig. 2a)[19–23]. SR2211 and GSK805 have been evaluated for their therapeutic potential in suppression of Th17 cell-mediated autoimmune disease models[22,24]. By combining the structural features of SR2211 and GSK805 and structure-based optimization, we developed compound XY018 that inhibited ROR-γ constitutive activity in 293T cells with high potency (EC_{50}, 190 nM) (Fig. 2a; Supplementary Fig. 2a–d). Molecular docking demonstrated that XY018 may bind to the ROR-γ hydrophobic LBD through several conserved hydrogen bonds and hydrophobic interactions. For example, the phenyl group in the middle likely forms a π-π interaction with the side chain of Phe378 of the LBD, while the amide group can form a direct hydrogen bond with Phe377. The nitro group and hydroxyl group at the two ends may form hydrogen bonds with Glu379 and His479,

respectively. Molecular dynamics simulation demonstrated that the ROR-γ-XY018 complex is very stable with these interactions (Supplementary Fig. 2e–f).

Given the crucial function of ROR-γ in prostate cancer cells *in vitro*, we examined whether its antagonists possess any growth-inhibitory effect. All of the ROR-γ antagonists tested inhibited PCa cell line growth with higher potency than ENZ (Fig. 2b and Supplementary Fig. 3a, b, c). Consistent with our data showing different expression patterns of ROR-α and ROR-γ, a ROR-α-selective antagonist SR3335[25] did not significantly inhibit CRPC cell line growth. Moreover, strong growth inhibition by XY018 and SR2211 was observed in other AR-positive PCa cell models including 22Rv1, VCaP, LNCaP, LAPC4 and PC346C (Supplementary Fig. 3a, b, c). No significant growth inhibition by the ROR-γ antagonists was seen in non-malignant human prostate cell RWPE1, normal human fibroblasts IMR90, or AR-negative PCa cells at the concentrations tested (Supplementary Fig. 3b, c). Consistent with the induction of apoptosis by ROR-γ gene knockdown, treatment of C4-2B and 22Rv1 cells with XY018 and SR2211 reduced colony formation and increased apoptosis (Fig. 2c–e and Supplementary Fig. 3d, e). In line with the cellular effects, XY018 and SR2211 suppressed the expression of key proliferation and survival proteins, including Myc (Fig. 2f and Supplementary Fig. 3f, g).

ROR-γ antagonists inhibit AR signaling

We next analyzed RNA-seq transcriptomes of C4-2B cells treated with the two structurally distinct antagonists, SR2211 and XY011, to identify gene programs affected by ROR-γ inhibition. Clustering of genes with expression significantly altered by either antagonist (relative to vehicle) showed a high degree of concordance in expression changes induced by the two ROR-γ inhibitors, with over 75% of genes either decreased (cluster 1) or increased (cluster 3) by both antagonists (Fig. 3a). Notably, genes of an AR activity signature derived from androgen-sensitive PCa cells and human tumors, which is of value in predicting clinical tumor response to androgen ablation therapy[26], constitute partly the two major clusters (cluster 1 and 3). Genes that are characterized as AR targets or androgen-induced genes were significantly inhibited by both antagonists. Conversely, the androgen-repressed genes were induced by the ROR-γ antagonists (Fig. 3a). Genes linked to androgen-induced cancer cell proliferation and survival were also contained in cluster 1 (e.g. *IGF1, RUNX2, UHRF1, MCM10, RRM2* and *CCNE2*) and 3 (e.g. *FAS, CDKN1B, DAB2IP and PTEN*) (Supplementary Fig. 4a). Moreover, the gene expression profiles induced by the antagonists significantly overlapped with that of anti-androgen ENZ (41% for SR2211, 38% for XY011 for down-regulated genes) (Fig. 3a and Supplementary Fig. 4b). Further examination by gene set enrichment analysis (GSEA) using the AR activity signature[26] revealed a robust disruption of AR gene programs by ROR-γ antagonists (Fig. 3b). The ROR-γ antagonists also inhibited the expression of genes preferentially up-regulated by AR-V727, and most of the genes within the 16-AR target gene set recently identified in human CRPC tumors[28] (Supplementary Fig. 4c, d). qRT-PCR verified that AR gene targets such as *KLK3, KLK2, NKX3.1*, and *FKBP5*, as well as genes linked to CRPC such as *CAMKK2*[29], and *ANCCA/ATAD2*[30] were inhibited by the ROR-γ antagonists and by ROR-γ knockdown (Fig. 3c and Supplementary Fig. 4e).

Inhibition of ROR-γ suppresses AR expression and genome binding

The prominent impact on AR-controlled gene programs by ROR-γ inhibition prompted us to investigate whether ROR-γ controls the expression and/or function of AR. Indeed, ROR-γ knockdown suppressed the mRNA and protein expression of AR full-length and AR-Vs/7 in C4-2B and VCaP cells. The ROR-γ antagonists (XY018, SR2211 and XY011) also inhibited the expression of AR and AR-V7 in a dose-dependent manner (Fig. 4a, b and Supplementary Fig. 5a, b). Similar dose-dependent inhibition was observed in other AR-positive cancer cell lines including 22Rv1, LAPC4 and PC346C (Supplementary Fig. 5c). Conversely, ROR-γ overexpression significantly increased AR expression in LNCaP cells (Supplementary Fig. 5d). Consistent with the results from cell models, in multiple data sets from human CRPC tumors, the expression of ROR-γ mRNA correlated strongly not only with AR expression but also with a CRPC AR-signature[28] (Supplementary Fig. 5e, f).

To assess the ROR-γ antagonist effect on AR function, we performed anti-AR ChIP-seq using C4-2B cells treated with 5 μM SR2211 for 24 hours; this caused a significant but incomplete suppression of AR expression (Supplementary Fig. 6a). SR2211 treatment reduced genome-wide AR binding to its target loci as well as genome-wide abundance of histone 3 lysine 27 acetylation (H3K27ac) (Fig. 4c and Supplementary Fig. 6b). AR binding at enhancers and/or promoters of targets such as *KLK2, KLK3, CAMKK2, NKX3.1, FKBP5* and *ANCCA/ATAD2* was almost completely eliminated by SR2211 (Fig. 4c, **right panel** and Supplementary Fig. 6c). Similar inhibition of AR binding was also seen with antagonist XY018 in ChIP-qPCR analysis (Fig. 4d). In line with the loss of AR occupancy, transcriptional activation-linked histone marks including H3K27ac and H3K4me2/3 were significantly reduced at KLK3 promoter and enhancer. As expected, RNA polymerase II (Pol-II) recruitment at the target promoters was also reduced (Fig. 4e and Supplementary Fig. 6d, e). Consistent with the effects of SR2211, knockdown of *ROR-γ* showed similar inhibitory effects on AR binding and associated histone marks (Supplementary Fig. 6f). The overall genome-wide distributions of H3K4me2 and H3K4me3 marks as well as Pol-II peaks were not markedly affected by SR2211 (Supplementary Fig. 6g), indicating that ROR-γ inhibition on H4K3me2/3 and Pol-II is target locus-specific.

The ROR-γ-selective antagonists (SR2211, XY018 and XY011) were identified based on the unique pocket structure of ROR-γ LBD. Nevertheless, to rule out the possibility that the antagonists act directly through AR, we performed a reporter gene assay. In a multimerized ARE-driven reporter that can be activated by synthetic androgen R1881 and repressed by anti-androgen ENZ, the three ROR-γ antagonists, at up to 10 μM, did not influence R1881-induced AR activity (Supplementary Fig. 7a). Moreover, molecular docking demonstrated that although XY018 could snugly dock into the ROR-γ ligand binding pocket, it simply cannot be accommodated by the AR ligand binding pocket due to the relatively short length of the pocket (Supplementary Fig. 7b).

To provide further evidence that the ROR-γ antagonists act through suppression of AR expression, we performed AR rescue experiments. First, we ectopically expressed a LBD-truncated form of AR in LNCaP cells and found that the growth inhibition by the antagonists was effectively mitigated in the cells while the endogenous AR was suppressed

(Supplementary Fig. 7c). Next, we performed a reporter assay with a 5.8 kb KLK3 regulatory sequence-linked luciferase gene. Results in Supplementary Fig. 7d shows that both the androgen-independent and androgen-stimulated activities of endogenous AR were strongly inhibited by the ROR-γ antagonists likely due to the suppression of AR expression. However, AR ectopic expression effectively blocked the inhibition by the antagonists. In contrast, the anti-androgen ENZ was still effective in blocking activity of the ectopic AR. Together, our results strongly suggest that the ROR-γ antagonists, acting through ROR-γ, effectively suppress the aberrant AR expression and function.

ROR-γ directly controls AR gene expression

The potent inhibition of AR expression by ROR-γ knockdown or antagonists led us to an examination whether ROR-γ directly controls AR gene transcription. ROR-γ binds DNA with specific sequence motifs AA/TNTAGGTCA (the classic RORE motif) or CT/AG/AGGNCA (the variant RORE motif)[13, 31]. In C4-2B cells, ChIP-qPCR of regions containing over 20 putative ROREs across the 250 kb AR locus demonstrated that ROR-γ bound to a site in the first exon (2.3 kb downstream of AR TSS) (Fig. 5a). The site contains sequences matching the variant RORE motif. When cells were treated with the ROR-γ antagonist SR2211, ROR-γ binding was reduced (Fig. 5a).

To examine the function of the putative RORE-containing site in mediating ROR-γ regulation of the AR gene, we used a lentiviral CRISPR-Cas9 editing system to first delete the site with two sets of sgRNAs in C4-2B cells (Fig. 5b, c and Supplementary Fig. 8a). Since the dependency of highly elevated AR for the cell proliferation and survival prevented us from expanding cell clones with genome editing-reduced AR, we analyzed heterogeneous populations of cells, some of which were edited and some of which were likely not. We found that even deletion in about half of the cell population (estimated from the PCR products of the wild type and deleted alleles in Fig. 5c, **left**) resulted in a significant reduction in the abundance of AR transcripts, which were detected by the upstream primers P1 and P2 (Fig. 5d). Next, we treated the editing-heterogeneous cell populations with the ROR-γ antagonists and analyzed AR transcripts with primers P3 and P4. As expected, abundance of transcripts from the WT allele was reduced by the three antagonists. In contrast, in the same samples, transcript levels from the deleted alleles were not significantly altered by any of the antagonists (Fig. 5e and Supplementary Fig. 8b), indicating that the site is required for ROR-γ antagonist-mediated inhibition of AR transcription. Moreover, as expected from the frameshiting effects caused by indels, the three sgRNAs, when used singularly, caused a “knock-out” effect on AR protein expression (Supplementary Fig. 8c). Importantly, sgRNA-2, the only one that could be designed to cause indel type of alterations adjacent to the RORE sequence, also significantly inhibited AR mRNA expression while the other two did not (Supplementary Fig. 8c). Finally, we performed reporter gene assays with the RORE and found that it was highly responsive to ROR-γ-mediated transactivation. Mutations in the core RORE sequence or deletion of ROR-γ C-terminal, AF2 transactivation domain completely abrogated the AR-RORE-dependent activation. The three ROR-γ antagonists suppressed the activation in a dose-dependent manner (Fig. 5f). Moreover, we observed a tight correlation between inhibition of ROR-γ activity (in 293T cells), inhibition

of AR expression (in C4-2B) and inhibition of proliferation (in C4-2B) (Supplementary Fig. 8d, e).

ROR-γ activates gene transcription through association with co-factors such as p160/SRC/NCoA family members[32]. Indeed, SRC-1 and SRC-3/ACTR occupied the AR-RORE site. Furthermore, their binding was strongly reduced by ROR-γ antagonism or knockdown (Fig. 5g; Supplementary Fig. 8f), indicating that the SRCs were recruited to the site via ROR-γ. Knockdown of SRC-1 and ACTR, but not SRC-2, individually or in combination, decreased AR mRNA and protein expression. Treating cells with bufalin, a cardiac glycoside inhibitor that was recently shown to selectively degrade SRC-1 and ACTR in cancer cells[33], also resulted in a dose-dependent inhibition of AR expression (Supplementary Fig. 8g, h). Next, we assessed the impact of ROR-γ inhibition on the local chromatin. Treatment with SR2211 significantly reduced the abundance of the gene activating marks H3K4me3 and H3K27ac at the RORE site and AR promoter (Fig. 5g; Supplementary Fig. 8i). Consistent with the reduction of AR transcripts, Pol-II occupancy at AR promoter and the RORE site was significantly inhibited by ROR-γ inhibition.

ROR-γ antagonists inhibit CRPC tumor growth

We next evaluated the effects of ROR-γ antagonists on prostate cancer tumor growth. Given the heterogeneity of PCa, we generated xenografts using PCa cell lines with distinct features (e.g. C4-2B which expresses AR with mutated LBD, VCaP with amplified AR gene and AR-V7, 22Rv1 which express high levels of multiple AR variants, and AR-negative PC3). In mice bearing the three AR-positive tumor models including ENZ-resistant 22Rv1, 5 mg/kg intraperitoneal injection of SR2211 (5 times/week when tumors reach approximately 100 mm^3) stopped tumor growth (Fig. 6a, b; Supplementary Fig. 9a). Tumor growth inhibition was also observed when using the other antagonists XY018 and XY011 as well as shRNA knockdown of ROR-γ in these models (Supplementary Fig. 9b–e). Moreover, in an orthotopic model of PCa, treatment with SR2211 suppressed tumor growth (Suppementary Fig. 9f–h). In line with a lack of significant effect on the growth of PC3 cells in vitro (Fig. 2c), SR2211 did not suppress growth of PC3-derived xenograft tumors (Supplementary Fig. 9i).

Notably, expression of AR and AR targets were markedly inhibited whereas tumor cell apoptosis measured by cleaved caspase-3/7 was strongly induced by SR2211 (Fig. 6c). ChIP analysis of xenograft tumors showed that SR2211 treatment blocked ROR-γ binding to the AR-RORE and AR binding to KLK3 as well as H3K27ac enrichment (Supplementary Fig. 10). Moreover, in a VCaP-derived mouse model of castration-resistant PCa, the antagonist SR2211 alone, at 5 mg/kg, significantly inhibited CRPC tumor growth whereas ENZ alone, at 10 mg/kg, did not. Co-administration of the two resulted in persistent suppression of tumor growth, indicating that the ROR antagonist can sensitize CRPC tumors to ENZ (Fig. 6d). As previously reported[34,35], VCaP xenograft tumors result in micrometastasis in mice. SR2211 treatment inhibited metastasis to the femur and liver (Fig. 6e).

Like ENZ, the ROR-γ antagonists were well tolerated, based on the weight of the animal body and vital organs, and their general behavior (Supplementary Fig. 9a–d, 9j, 11a). Consistent with ROR-γ being an adipogenesis factor[36], the antagonist reduced the amount

of the white adipose tissue. Thus, the antagonists can block CRPC tumor growth and effectively sensitize tumors to ENZ, without overt toxicity. Interestingly, unlike ENZ, the antagonists did not display any discernable effect on the growth of androgen-responsive tissues such as mouse prostate and testis or AR expression in the tissue (Supplementary Fig 11b–d). Analysis of two non-malignant human prostate epithelial cells showed that the antagonists did not have any significant effect on endogenous AR expression (Supplementary Fig. 12a). To explore the underlying mechanism, we performed ChIP and found no detectable ROR-γ binding to the RORE-corresponding site in mouse prostate tissue and the two human cell lines (data not shown). Immunoblotting revealed very low level of ROR-γ expression in the human cells (Supplementary Fig. 12a). Sequence comparsion showed that the corresponding site of mouse AR gene lacks a functional RORE[13,14](Supplementary Fig. 12b). Together, our results suggest that the ROR-γ antagonists can inhibit AR expression specifically in tumor cells and not in nonmalignant cells.

DISCUSSION

The most common mechanism driving CRPC development appears to be reactivated AR signaling mediated by high levels of AR and its variants in PCa. Therapeutically actionable means to effectively suppress AR expression is still lacking. Our study not only demonstrates that ROR-γ acts as a key determinant of AR gene expression but also provides a unique opportunity for effective therapeutic intervention of CRPC. We found that ROR-γ directly stimulates AR gene transcription by binding to an exonic RORE and partly through the NR coactivators SRC-1 and SRC-3. Although SRCs and other AR coactivators likely play important roles in prostate cancer[37–41], they have not been shown to be directly involved in AR gene overexpression. We demonstrate here that small molecule antagonists of ROR-γ potently disrupt ROR-γ and the SRC binding to the AR locus, reduce the local activating histone marks and effectively suppress AR expression *in vitro* and *in vivo*. Transcription factors such as E2F1, LEF/TCF, and NF-κB can activate AR expression whereas others were shown to suppress it[42–46]. It is possible that ROR-γ also acts in concert with them or other factors.

The alternatively spliced variants of AR in tumors treated by anti-androgens and CYP17 inhibitors (e.g. ENZ and ABI) is linked to therapeutic resistance and metastasis[47]. Recently, agents targeting the AR NTD, an intrinsically unstructured/disordered domain, or enhancing degradation of the full-length AR protein are in development[5–8]. We propose that targeting ROR-γ with its selective antagonists effectively inhibits the expression of AR variants such as AR-V7 as well as AR full-length, at the gene transcriptional level, therefore mitigating or even eliminating the root cause of the problem, namely the highly elevated AR gene transcripts and proteins. The ROR-γ antagonists potently inhibited growth of different AR-positive tumors including those with AR gene amplification and/or high levels of AR variants, in mice. Notably, tumors that are resistant to ENZ are sensitive to the antagonists (either alone or in combination with ENZ), suggesting that ROR-γ targeting can have a broad clinical utility in PCa. The ROR-γ antagonists' effect on AR expression, instead of on AR LBD function, may also offer other therapeutic advantages over anti-androgens. Indeed, unlike anti-androgens that suppress the growth and function of normal androgen-responsive

tissues such as testis and prostate, the ROR-γ antagonists do not show any significant impact on the size of the mouse tissues or AR expression in the tissues and human non-malignant prostate cells, because of the lack of ROR-γ function. This tumor-specific effect of the antagonists is likely attributable to tumor cell addiction to elevated levels of AR and tumor cell-specific control of AR by ROR-γ.

The impact of ROR-γ antagonists on AR gene programs in CRPC cells appears extensive, encompassing AR targets that are up-regulated, down-regulated or persistently expressed in CRPC tumors[28]. However, the overall impact on CRPC tumors is unlikely limited to AR and its programs. Inflammatory tumor microenvironment is believed to promote CRPC and tumor metastasis through production of cytokines such as IL-17[48,49]. Thus, ROR-γ in tumor-inflitrating lymphocytes could play an important role. Therefore, targeting ROR-γ can stop tumor growth and metastasis possibly through blocking multiple pathways including aberrant AR signaling. As more potent and orally bioavailable ROR-γ antagonists are being developed and entering clinical trials for human autoimmune diseases, our findings here may have immediate implications on development of a new generation of prostate cancer therapeutics.

ONLINE METHODS

Cell culture

LNCaP, C4-2B, 22Rv1, PC-3, and PC346C prostate cancer cells were cultured in RPMI1640, VCaP, HEK293T and human fibroblast IMR90 cells were in DMEM, LAPC-4 was in Iscove's MEM (all from Corning), and RWPE-1and PZ-HPV-7 were in Keratinocyte Serum Free Medium (K-SFM) (Invitrogen) with the supplements. All the culture media except for RWPE-1 and PZ-HPV-7 were supplemented with 10% FBS (Hyclone or Gemini) except indicated otherwise. For experiments, C4-2B cells were cultured in RPMI supplemented with 9% charcoal-dextran-stripped (cds)-FBS plus 1% regular FBS (to mimic the CRPC condition) unless indicated otherwise. 22Rv1 cells were cultured in RPMI supplemented with 10% cds-FBS. LN/TC-AR cells that inducibly express a C-terminally truncated variant of androgen receptor were derived from LNCaP cells as previous described[50]. Cells were grown at 37°C in 5% CO2 incubators. LNCaP, VCaP, 22Rv1, PC-3, 293T, IMR90, PZ-HPV-7 and RWPE-1 were from ATCC. C4-2B was from UroCor Inc. (Oklahoma City, OK). LAPC4 and PC346C were kindly provided respectively by Dr. Charles Sawyers (MSKCC, New York) or by Dr. Adrie van Bokhoven (University of Colorado). The prostate cancer cell lines were recently authenticated by ATCC using STR profiling. Cell lines were regularly tested being negative for mycoplasma.

Chemicals

Sources for chemicals are as follows: SR2211, Calbiochem and TOCRIS; SR1555 and SR3335, Cayman. Information on XY018 and XY011 is provided below or described before[21]. Other chemicals are from Sigma unless indicated otherwise.

qRT-PCR and immunoblotting analysis

Total RNA was isolated from cells in 6-well or 10-cm plates or from xenograft tumors, and the cDNA was prepared, amplified and measured in the presence of SYBR as previously[51]. Briefly, the fluorescent values were collected and a melting curve analysis was performed. Fold difference was calculated as described previously[51]. The experiments were performed at least three times with data presented as mean values ± s.d. Cell lysates were analyzed by immunoblotting with antibodies specifically recognizing ROR-γ, AR, AR-V7 and the indicated proteins. The PCR primers and all the antibodies used in this study are described in the Supplementary table 1 and 2.

Analysis of ROR mRNA expression, genetic alterations and association with CRPC AR signature in clinical tumors

Publicly available prostate cancer expression data sets GSE6919, GSE35988, GSE6811 and GSE70768 from previous studies[52–55] were downloaded from GEO at http://www.ncbi.nlm.nih.gov/geo/. The datasets contain gene expression profiles of benign, primary, metastatic and/or CRPC tumor samples. Normalized probe set expression for RORs were compared between the different tissue/tumor groups by a two-tailed *t* test for significance. Computations were conducted in R statistical package (http://www.r-project.org/). For genetic alterations of ROR genes, data from a recent genomics study[18] at cBioPortal for Cancer Genomics (http://www.cbioportal.org) was interrogated and OncoPrint displays of gene alterations were presented. Expression correlation between ROR-γ and AR in tumors was assessed by computing the Pearson correlation coefficient (*r*) and a two-tailed *t* test for significance. For correlation between ROR-γ and the AR signature activity, the expression of the 150 CRPC AR-signature genes[28] is summarized as a single expression profile as previous reported[56] before applied to computation of the Pearson correlation statistics.

Immunohistochemistry (IHC) and statistics analysis

IHC was performed as previously described[51,57] with the following modifications. Antigen retrival for sections of tissue microarrays (TMA PR803b from Biomax.US) was performed in a pressure cooker. The slides were then incubated with anti-ROR-γ monoclonal antibody (AFKJS-9, eBioscience) at 1:50 dilutions overnight at 4°C, followed by incubations with biotinylated secondary antibody and the ABC reagents in the Vectastain Elite kit and counter-stained with hematoxylin. The TMA contained specimens from 70 cases of prostate cancer with information provided for most of the cases on stage, Gleason scores and TNM grading. The percentage of positive nuclear staining was scored as follows: 0% – <5%, score 0; 5% – <10%, score 1; 10% – 50%, score 2; >50%, score 3. Differences and correlations in immunostaining among groups were analyzed with the χ^2 test.

Cell viability, apoptosis and growth assays, and colony formation

For cell viability, cells were seeded in 96-well plates at 1500–2500 cells per well (optimum density for growth) in a total volume of 100μl media. Serially diluted compounds in 100μl of media were added to the cells 12 hours later. After 4 days of incubation, Cell-Titer GLO reagents (Promega) were added and luminescence was measured on GLOMAX microplate

luminometer (Promega), according to the manufacturer's instructions. All experimental points were set up as sextuplicate as biological replication and the entire experiments were repeated three times. The data are presented as percentage of viable cells with vehicle treated cells set as 100. The estimated *in vitro* IC_{50} values were calculated using GraphPad Prism 6 software.

For apoptosis, Terminal deoxynucleotidyl transferase–mediated dUTP nick end labeling (TUNEL) was performed by using *in situ* cell death detection kit (Roche) as previously described[57]. The results are expressed as a percentage of apoptotic cell number/total cell number. Caspase-3/7 activity was measured using a luminescent caspase-Glo 3/7 assay kit (Promega Corporation, Madison, USA) following the manufacturer's instructions. For cell growth, cells were seeded in 6-well plates at 2×10^5 per well and treated as indicated. Total viable cell numbers were counted using a Coulter cell counter. For colony formation, 800 cells were seeded in a well of 6-well plates and cultured for 14 days with the medium changed every 3 days. When the cell clone grew visible, the medium was removed and the cells were fixed with 10% formalin for 10 minutes. Then the plates were washed with PBS for two times and the cell colonies were stained with 0.2% crystal violet (in 10% formalin) for 15 minutes. The numbers of cell colonies were counted after washed 5 times by PBS. The above assays were performed in triplicates and the entire experiments were repeated three times.

ROR-γ shRNA and overexpression lentivirus production and siRNA transfection

Lentiviral plasmids encoding shRNA targeting ROR-γ/RORC (TRCN0000033655 and TRCN0000033658) were purchased from Sigma. Non-targeting control shRNA were used as described[51]. For ROR-γ overexpression, human ROR-γ cDNA in pLX304 (DNASU) was amplified and cloned into a modified pLX304 vector with a V5 tag at the receptor N terminus. Lentiviral particles were produced in 293T cells after co-transfection of the above lentivirus vectors, psPAX2 and pMD2.G in 10 cm dishes, as described[51]. siRNAs for gene knockdown were purchased from Dharmacon. The siRNA target sequences for ROR-γ and different SRCs are listed in supplementary table 3. Transfections were performed with OptiMEM (Invitrogen) and Dharmafectin#1 (Dharmacon) following manufacturer's instruction.

Reporter constructs and reporter gene assays

Transient transfection and reporter gene assays were performed as previously described[51] with following modifications. ARE reporter gene assays were performed by transfecting 22Rv1 cells with 5 × ARE-tk-luc, pcDNA3.1-hAR and pCMV-β-gal for normalization. For transfection with constructs omitted for specific gene expression, corresponding empty vectors were used to ensure equal amount of total DNA used. Briefly, 22Rv1 cells seeded in 96- well plates in hormone-deprived medium supplemented with 10% cds-FBS (Hyclone) were transfected with lipofectamine 2000 (Life technology, Carlsbad, CA, USA) and the indicated plasmid DNA. Cells were then treated at 12 hours after transfection with 3 nm R1881, indicated concentrations of ROR-γ antagonists or ENZ for another 24 hours before harvested for β-gal and luciferase assays. For RORE reporter gene assays, 4 × AR-RORE-tk-luc was constructed by inserting four copies of the newly identified AR-RORE

TTCTGGGTCA into tk-luciferase reporter vector. AR-RORE mutant form (AR-RORE mut) contains sequences mutated from TTCTG**GGTC**A to TTCTG**AACG**A. Cells (HEK293T) were co-transfected with CMX-ROR-γ or CMX-ROR-γΔH12 expression vector and the RORE-tk-luc reporter plasmid as indicated using Lipofectamine 2000 (Life technology, Carlsbad, CA, USA). After 12 h incubation, cells were treated with vehicle or ROR-γ antagonists as indicated for another 24 hours. For Gal4-driven reporter assays, 293T cells were transfected with Gal4-ROR-γ LBD and pGL5-luc reporter. The luciferase and β-galactosidase were then analyzed with a Luciferase Assay Substrate (Promega) and Luminescent β-galactosidase Detection Kit II (Clontech). All transfections were performed in triplicate, and each experiment was repeated at least three times.

CRISPR/Cas9 sgRNA design, lentivirus production and PCR-based assay to detect genomic deletions

sgRNAs were designed using the MIT CRISPR design software (http://crispr.mit.edu). Oligos corresponding to the sgRNAs were synthesized and cloned into lentiCRISPR v2 vectors following lentiCRISPRv2 and lentiGuide oligo cloning protocol (Addgene, plasmid#52961). sgRNA sequences are as follows: GFP: GGGCGAGGAGCTGTTCACCG; AR-RORE#1: CTGGCGAGCCTGCATGGCGC; AR-RORE#2: GTGCAGCGGGACCCGGTTCT; AR-RORE#3: ACTCTCTTCACAGCCGAAGA. Lentiviral particles were produced in 293T cells as described above. C4-2B cells were plated at 2×10^5 cells per well in 6-well plates. Sixteen hours later, 1 ml of virus-containing supernatant with 10 ng polybrene was added to the cells. After 4 to 6 hours, medium was changed to regular medium and cultured for another 72 hours. Genomic DNA was isolated from cells using the PureLink Genomic DNA kit (Life technology). PCR was performed using indicated primers flanking the sgRNA target sites. PCR products from deleted alleles were purified by running agarose gel and were ligated into plasmids using pGEM-T Easy Vector Systems (Promega). Plasmid DNA was purified from single bacterial colonies by mini-prep kit (Qiagen) and sequenced by GENEWIZ (Davis, California) using Sanger sequencing method.

Analysis of AR mRNA expression in cells treated with CRISPR/Cas9-sgRNA lentivirus

Cells were infected with the CRISPR/Cas9 sgRNA lentiviruses as above and cultured for 2 days. ROR-γ antagonists or vehicle were then added and cells were cultured for another 2 days. Total RNA was extracted by TRIzol and reverse transcribed. Semi-quantitative RT-PCR was performed using the template cDNA generated and indicated primers. PCR products were separated on agarose gels. Quantification of the bands was performed as previously reported[58]. Band intensity was expressed as relative absorbance units and normalized to GAPDH.

RNA-seq data analysis

C4-2B cells were treated with vehicle or the antagonists XY011 (5 μM) and SR2211 (5 μM) or ENZ (20 μM) for 48 hours before RNA extraction. RNA-seq libraries from 1μg total RNA were prepared using Illumina Tru-Seq RNA Sample, according to the manufacturer's instructions. Libraries were validated with an Agilent Bioanalyzer (Agilent Technologies,

Palo Alto, CA). Sequencing was performed on an Illumina HiSeq 2000 sequencer at BGI Tech (Hong Kong). The FASTQ-formatted sequence data were analyzed using a standard BWA-Bowtie-Cufflinks workflow[59–61]. In brief, sequence reads were mapped to the reference human genome assembly (Feb. 2009,GRCh37/hg19) with BWA and Bowtie software. Subsequently, the Cufflinks package[62] was applied for transcript assembly, quantification of normalized gene and isoform expression in RPKM (Reads per kilobase per million mapped reads) or FPKM (fragments per kilobase of exon model per million mapped reads), and testing for differential expression (Cuffdiff). To avoid spurious fold levels due to low expression values, only those genes with expression RPKM or FPKM values > 1 for either the vehicle/control cell, or the antagonist treated cells (but need not to be both), are included. The expression change of at least 1.5 fold up or down was clustered with K-mean clustering algorithm in Cluster software[63]. The cluster was displayed with TreeView.

GSEA analysis

GSEA was performed using the Java desktop software (http://www.broadinstitute.org/gsea) as described previously[64]. Genes were ranked according to the shrunken limma $\log_2$ fold changes and the GSEA tool was used in 'pre-ranked' mode with all default parameters. Previous reported AR activity signature genes[26] were used in the GSEA analysis.

ChIP-qPCR analysis

ChIP-qPCR analysis was performed as described previously[51]. The antibodies used for ChIP assay are AR (Santa Cruz; sc-815); RNA Pol-II (Santa cruz; sc-899); H3K4me2 (Abcam ab32356); H3K4me3 (Abcam; ab8580); H3K27ac (Abcam; ab4729); H3 (Active Motif; #39163); p300 (Santa Cruz; sc-585); SRC-1 (Santa Cruz; sc-8995); SRC-3/ACTR[65], and IgG (Santa Cruz; sc-2027). Anti-RORγ rabbit serum was generated by Covance using purified GST-human RORγ fragment (amino acids 79–301) expressed in E.coli. PCR primers used in the ChIP assays were listed in the Supplementary table 2. ChIPs were performed with each experimental point in triplicate, and each experiment was repeated three times.

ChIP-seq and data analysis

C4-2B cells were treated with vehicle or SR2211 (5 μM) for 24 hours before harvested for ChIP-seq. ChIP-seq experiments were performed as described[66]. Anti-AR ChIP-seq was repeated in two independent experiments. Antibodies used were against AR (Santa Cruz; sc-815); RNA Pol II (Santa cruz; sc-899); H3K4me2 (Abcam ab32356); H3K4me3 (Abcam; ab8580); H3(acetyl K27) (Abcam; ab4729). Libraries were quantified with the Bioanalyzer 2100 (Agilent) and sequenced on the Illumina HiSeq 2000 Sequencer (BGI, Hong Kong). Sequencing tags were mapped against the Homo sapiens (Human) reference genome (hg19) using Bowtie 2[67]. Uuniquely mapped tags were used for peak calling by MACS(2.1.0)[68] to identify regions of ChIP-Seq enrichment over background. A q value threshold of enrichment of 5×10^{-2} was used for all data sets. Normalized genome-wide signal coverage tracks from raw read alignment files were built by MACS2, UCSC tools (http://hgdownload.cse.ucsc.edu/admin/exe/linux.x86_64/bedGraphToBigWig/bedClip) and bedTools (http://code.google.com/p/bedtools/). Visualization of ChIP-seq singnal at enriched

genomic regions(avgprof and heatmap) was achieved by using ngs.plot (https://github.com/shenlab-sinai/ngsplot).

Xenograft tumor models and chemical compound treatments

Four-week-old male SCID C.B17 mice (for C4-2B and VCaP) or BALB/c nu/nu athymic mice (for 22Rv1 and PC-3) were purchased from Harlan Inc. For establishing tumors, 2×10^6 cells were suspended in total of 100 μL PBS/Matrigel (1:1) and implanted subcutaneously into the dorsal flank on both sides of the mice. Animal group size of six or more was estimated to have a high statistic power, based on power calculation (http://www.biomath.info/power/) and previous studies involving the same xenograft models[34,69]. When the tumor volume was approximately 80 mm^3, the mice were randomized and then treated intraperitoneally (i.p.) with 100 μl of either vehicle or ROR-γ antagonists SR2211, XY018 or XY011/8K (in a formulation of 15% Cremophor EL, Calbiochem, 82.5% PBS, and 2.5% DMSO) for five times per week. Tumor growth was monitored by calipers with volume calculated using the equation: (π/6 (length × width2)). Body weight during the course of the study was also monitored. At the end of the studies mice were killed and tumors were dissected and weighed. Additionally, prostate, seminal vesicle, testis, kidney, heart, lung, liver, epididymal fat pad and spleen were harvested and weighed. To assess the effect of combining ROR-γ antagonists and ENZ on the growth of castrated-resistant VCaP xenografts (CRPC-VCaP), first, SCID C.B17 mice were injected with VCaP cells as above to establish the tumors. Then, mice bearing tumors of approximately 180 mm^3 were surgically castrated. They were then observed for tumor regression. Once tumors grew back to the pre-castration size, mice were randomized and treated with vehicle, 5 mg kg^{-1} SR2211, 10 mg kg^{-1} ENZ or a combination of 5 mg kg^{-1} SR2211 and 10 mg kg^{-1} ENZ. ENZ was given by oral gavage as previously described[69] and SR2211 was administered i.p as above. Mice were exluded from the study if bearing no tumor or tumor with size twice larger or smaller than the mean, at the time of randomization.

To assess the effect of ROR-γ antagonists on the growth of orthotopic prostate tumors, C4-2 cells suspended in Matrigel as above were injected orthotopically into SCID C.B17 mice. To monitor tumor growth, mice were bled and serum PSA levels were measured using PSA (human) ELISA kit (Abnova). When serum PSA were detectable, the mice were randomized into different groups for the treatment. To assess the effect of ROR-γ knock down on tumor growth, C4-2B cells infected with lentivirus encoding control shRNA or shRNA targeting ROR-γ were injected subcutaneously into both sides of the dorsal flank of mice. Tumor growth was monitored weekly by calipers. Tumor volumes were measured in a blinded fashion (to treatment groups). The procedures were approved by the Institutional Animal Care and Use Committee of University of California Davis.

Statistical Analysis

Cell culture-based experiments were performed three times or more with assay points triplicated or sextuplicated, as indicated. The data are presented as mean values ± s.d. from three independent experiments. Statistics analysis was performed using two-tailed Student's *t* tests to compare means. $p < 0.05$ was considered significant.

Molecular docking & molecular dynamics simulation

Schrödinger 2014 Suite was used to predict the potential binding mode of ROR-γand its ligands. The crystal structure of ROR-γ LBD in complex with antagonist (PDB code: 4QM0.pdb) was used as the reference structure in the docking study. Protein structure preparation for docking studies included water deletion, hydrogen atom addition and protonation state adjustment. All of the ligand and protein preparation were performed in Maestro (version 9.9, Schrödinger, LLC, New York, NY, 2014) implemented in the Schrödinger program (http://www.schrödinger.com). In this study, ligands were prepared using the Ligprep module to obtain energy minimized 3D structures, which were then docked into ligand binding pocket with the Glide molecular docking program (version 6.4, Schrödinger, LLC, New York, NY, 2014) using the Glide SP, and Glide XP modes. For all of the methods, Glide docks flexible ligands into a rigid receptor structure. Final ranking from the docking was based on the docking score, which combines the Epik state penalty with the Glide Score. Finally, the binding poses with the top glide score (20 poses) were clustered and selected for further visual evaluation and molecular dynamics simulations.

Molecular dynamics (MD) simulations were conducted by using AMBER 14 program. The starting coordinates were obtained from docking results. For ligand coordinates, top scored representative poses of each cluster were chosen. For protein coordinates, the protein preparation panel in Schrodinger 2014 Suite was applied to assign the protonation states and orientations of residues, which was then further processed by using LEaP module in Amber program. Parameters of compounds were prepared by AM1-bcc model and the other parameters were assigned from the AMBER GAFF force field using ANTECHAMBER. Topology and parameter files for the protein, ligand and complex were generated using the LEaP module in AMBER 14. TIP3PBOX water molecules were added in cube periodic boxes, which were 10 Å × 10 Å × 10 Å. To ensure overall neutrality of the system, appropriate Na^+ and Cl^- were added at physiological concentration in the box. For each system, energy minimization and MD simulation were carried out using the GPU version of the PMEMD program in AMBER 14 program. The MD simulations were performed for up to 200 ns for each complex system. The coordinates of the complexes were saved every 2 ps, those snapshots were taken in production run for detailed analysis. Trajectories were analyzed using the PTRAJ module in Amber 14.

AlphaScreen Assay

The human ROR-γ LBD (residues 262–507) was expressed as a His6-fusion protein using the pET24a expression vector (Novagen, Madison, WI) as described in reference[11]. Interactions between ROR-γ and ligands were assessed by luminescence-based AlphaScreen technology (Perkin Elmer) using a histidine detection kit from PerkinElmer (Norwalk, CT). All of the reactions contained 100 nM receptor LBD bound to nickel acceptor beads (5 μg/mL) and 20 nM biotinylated SRC1-4 peptide bound to streptavidin donor beads (5 μg/mL) in the presence or absence of the indicated amounts of control compounds SR2211 or candidate compounds. The N-terminal biotinylated coactivator peptide SRC1-4 sequence was QKPTSGPQTPQAQQKSLLQQLLTE. Compound concentrations varied from 150 nM to 200 μM in the dose-response assay.

Thermal Shift Assay

All reactions were carried out using a CFX96 real-time PCR system (Bio-Rad). Protein were buffered in 10 mM of HEPES, pH 7.5, 150 mM of NaCl and 5% glycerol at a concentration of 7.5 μM. Compounds were added at a final concentration of 200 μM. All assays were set up in 20 μL final reaction volume in 96-well plate with 10× SYPRO Orange (Invitrogen) and incubated with compounds on ice for 30 mins. The samples were heated from 30 °C to 90 °C with a thermal ramping rate of 1 °C/min and the fluorescence signals were read out. ΔTm was recorded as the difference between the transition midpoints of sample and reference wells containing protein without ligand in the same plate.

Synthesis of N-(2'-fluoro-4'-(1,1,1,3,3,3-hexafluoro-2-hydroxypropan-2-yl) -[1,1'-biphenyl]-4-yl)-2-(2-nitrophenyl)acetamide(XY018)

Reagents and solvents were obtained from commercial suppliers and used without further purification. Flash chromatography was performed using silica gel (300–400 mesh). All reactions were monitored by TLC, using silica gel plates with fluorescence F254 and UV light visualization.^{1}H-NMR spectra were recorded on a Bruker AV-400 spectrometer at 400 MHz. Coupling constants (*J*) are expressed in hertz (Hz). Chemical shifts (δ) of NMR are reported in parts per million (ppm) units relative to internal control (TMS). The low- or high-resolution of ESI-MS was recorded on an Agilent 1200 HPLC-MSD mass spectrometer or Applied Biosystems Q-STAR Elite ESI-LC-MS/MS mass spectrometer, respectively.

To 2-fluoroaniline (6g, 54 mmol) in a pressure vessel was added hexafluoroacetone trihydrate (12.5 g, 56.7 mmol) and p-toluenelsuphonic acid (0.85 g, 5.4 mmol). The reaction mixture was stirred at 90°C for 12 hrs. After water was added, it was extracted with ethyl acetate and the organic layer was washed with saturated $NaHCO_3$solution and brine and dried over Na_2SO_4. The solid was filtered off and the filtrate was concentrated under reduced pressure. The resulting crude product was purified by silica gel chromatography with petroleum ether/ethyl acetate (10/1, v/v) to yield 2-(4-Amino-3-fluorophenyl)-1,1,1,3,3,3-hexafluoropropan-2-ol as white solid (4.45 g, 30 % yield).MS (ESI), m/z for $C_9H_6F_7NO$ ($[M+1]^+$): Calcd 277.14, found 278.0.

To a solution of 2-(4-amino-3-fluorophenyl)-1,1,1,3,3,3-hexafluoro propan-2-ol (4.45 g, 16.1 mmol) in DMF (100mL) was added concentrated HCl (18 mL, 73 mmol) and sodium nitrite (1.66 g, 24 mmol), dissolved in H_2O (20 mL) at 0 °C. The reaction mixture was stirred at 0°C for 30 min. Then potassium iodide (4 g, 24 mmol) was added in portions. The mixture was stirred at room temperature for overnight. Added ethyl acetate, washed with a saturated $NaHCO_3$solution and brine and dried over Na_2SO_4. The solid was filtered off, and the filtrate was concentrated under reduced pressure. The resulting crude product was purified by silica gel chromatography with petroleum ether/ethyl acetate (50/1, v/v) to yield 1,1,1,3,3,3-hexafluoro-2-(3-fluoro-4-iodophenyl)propan-2-ol (6.2 g, 96 % yield). ^{1}HNMR: (400 MHz, *d*-DMSO) δ 7.31 (d, *J* = 8.4 Hz, 1H), 7.48 (d, *J* = 1.6 Hz, 9.2 Hz, 1H), 8.05 (dd, *J* = 6.8 Hz, 8.4 Hz, 1H), 9.07 (s, 1H).

To a solution of 1,1,1,3,3,3-hexafluoro-2-(3-fluoro-4-iodophenyl) propan-2-ol (6.2 g, 16 mmol) in 1,4-dioxane (100 mL) and water (20 mL) was added (4-((tert-

butoxycarbonyl)amino)phenyl)boronic acid (4.2 g, 17.6 mmol), followed by addition of potassium carbonate (6.6 g, 48 mmol) and $Pd(PPh_3)_4$(0.9 g, 0.78 mmol), the vessel was purged with argon, sealed and heated to 80°C for 5 hrs. Added water, extracted with ethyl acetate, the organic layer was washed with brine and dried over Na_2SO_4. The solid was filtered off, and the filtrate was concentrated under reduced pressure. The resulting crude product was purified by silica gel chromatography with petroleum ether/ethyl acetate (20/1, v/v) to yield tert-butyl(2'-fluoro-4'-(1,1,1,3,3,3-hexafluoro-2-hydroxypropan-2-yl)-[1,1'-biphenyl]-4-yl)carbamate (5.35 g, 74 % yield). ^{1}H NMR (400 MHz, $CDCl_3$) δ 7.54 –7.44 (m, 6H), 7.40 (d, *J* = 8.4 Hz, 1H), 6.57 (s, 1H), 3.82 (s, 1H), 1.53 (d, *J* = 3.2 Hz, 9H).

To a solution of tert-butyl (2'-fluoro-4'-(1,1,1,3,3,3-hexafluoro-2-hydroxypropan -2-yl)-[1,1'-biphenyl]-4-yl)carbamate (5.35 g, 11.8 mmol) in DCM (50 mL) was added trifluoroacetic acid (7 mL, 96 mmol) dropwise at 0 °C. The reaction mixture was stirred at room temperature for 3 hrs and then concentrated under reduced pressure. Recrystallisation was then carried out in petroleum ether and ethyl acetate and 2-(4'-amino-2-fluoro-[1,1'-biphenyl]-4-yl)-1,1,1,3,3,3-hexafluoro propan-2-ol was isolated (3.8 g, 91% yield). ^{1}H NMR (400 MHz, *d*-DMSO) δ 8.91 (s, 1H), 7.61 (t, *J* = 8.4 Hz, 1H), 7.50 – 7.47 (m, 2H), 7.30 (d, *J* = 7.2 Hz, 2H), 6.65 (d, *J* = 8.4 Hz, 2H), 5.41 (s, 2H).

To a solution of 2-(2-nitrophenyl) acetic acid (56 mg, 0.31 mmol) in DCM (20 mL) was added HATU (213 mg, 0.56 mmol) and DIPEA (0.5 mL). The mixture was stirred at room temperature for 5 min, then added 2-(4'-amino-2-fluoro-[1,1'- biphenyl]-4-yl)-1,1,1,3,3,3-hexafluoro propan-2-ol (100 mg, 0.28 mmol). The reaction mixture was stirred at room temperature for 3 h. Added water, extracted with ethyl acetate, the organic layer was washed with brine and dried over Na_2SO_4. The solid was filtered off and the filtrate was concentrated under reduced pressure. The resulting crude product was purified by silica gel chromatography with petroleum ether/ethyl acetate (4/1, v/v) to yield N-(2'-fluoro-4'-(1,1,1,3,3,3-hexafluoro-2-hydroxypropan-2-yl)-[1,1'-biphenyl]-4-yl)-2-(2-nitrophenyl)acetamide (118 mg, 81% yield). ^{1}H NMR (400 MHz, $CDCl_3$) δ 8.09 (d, *J* = 8.4Hz, 1H), 7.94 (s, 1H), 7.66 (t, *J* = 7.6 Hz, 1H), 7.61 – 7.46 (m, 9H), 4.26 (s, 1H), 4.03 (s, 2H). MS (ESI), m/z for $C_{23}H_{15}F_7N_2O_4$ ($[M+1]^+$): Calcd 516.37, found 517.0.

Supplementary Material

Refer to Web version on PubMed Central for supplementary material.

Acknowledgments

We thank D. Wu, Q. Wang, D. Chen and J. Shen for their expertise in ChIP-seq, bioinformatics and critical comments. This work was supported in part by grants from the Bridge Program of UCD Research Office (to H-W. C.), the US National Institutes of Health (R01 CA206222 to H-W. C.) and US Department of Veterans Affairs, Office of R&D (I01 BX002237 to H-W. C.), the National Natural Science Foundation and Key Basic Research Program of China (Grant 81373325 and 973 Program Grant 2013CB910601 to Y. X.), the Howard Hughes Medical Institute and US National Institutes of Health (R01 DK057978 to R.M.E.), the US National Institutes of Health (R01 CA150197 and R01 CA165263 to H-J. K.), and the US Department of Defense (PC111467) and SU2C-AACR-PCF DT0812 (to C.P.E.).

References

1. Ferraldeschi R, Welti J, Luo J, Attard G, de Bono JS. Targeting the androgen receptor pathway in castration-resistant prostate cancer: progresses and prospects. Oncogene. 2015; 34:1745–1757. [PubMed: 24837363]
2. Karantanos T, et al. Understanding the mechanisms of androgen deprivation resistance in prostate cancer at the molecular level. European urology. 2015; 67:470–479. [PubMed: 25306226]
3. Watson PA, Arora VK, Sawyers CL. Emerging mechanisms of resistance to androgen receptor inhibitors in prostate cancer. Nature reviews. Cancer. 2015; 15:701–711. [PubMed: 26563462]
4. Mostaghel EA, Plymate SR, Montgomery B. Molecular pathways: targeting resistance in the androgen receptor for therapeutic benefit. Clinical cancer research : an official journal of the American Association for Cancer Research. 2014; 20:791–798. [PubMed: 24305618]
5. Myung JK, et al. An androgen receptor N-terminal domain antagonist for treating prostate cancer. The Journal of clinical investigation. 2013; 123:2948–2960. [PubMed: 23722902]
6. Lai KP, et al. New therapeutic approach to suppress castration-resistant prostate cancer using ASC-J9 via targeting androgen receptor in selective prostate cells. The American journal of pathology. 2013; 182:460–473. [PubMed: 23219429]
7. Liu C, et al. Niclosamide inhibits androgen receptor variants expression and overcomes enzalutamide resistance in castration-resistant prostate cancer. Clinical cancer research : an official journal of the American Association for Cancer Research. 2014; 20:3198–3210. [PubMed: 24740322]
8. Yu Z, et al. Galeterone prevents androgen receptor binding to chromatin and enhances degradation of mutant androgen receptor. Clinical cancer research : an official journal of the American Association for Cancer Research. 2014; 20:4075–4085. [PubMed: 24874833]
9. Malik R, et al. Targeting the MLL complex in castration-resistant prostate cancer. Nat Med. 2015; 21:344–352. [PubMed: 25822367]
10. Kojetin DJ, Burris TP. REV-ERB and ROR nuclear receptors as drug targets. Nature reviews. Drug discovery. 2014; 13:197–216. [PubMed: 24577401]
11. Zhao X, et al. Nuclear receptors rock around the clock. EMBO reports. 2014; 15:518–528. [PubMed: 24737872]
12. Zhang Y, Luo X-y, Wu D-h, Xu Y. ROR nuclear receptors: structures, related diseases, and drug discovery. Acta Pharmacol Sin. 2015; 36:71–87. [PubMed: 25500868]
13. Takeda Y, et al. Retinoic acid-related orphan receptor gamma (RORgamma): a novel participant in the diurnal regulation of hepatic gluconeogenesis and insulin sensitivity. PLoS Genet. 2014; 10:e1004331. [PubMed: 24831725]
14. Giguere V, et al. Isoform-specific amino-terminal domains dictate DNA-binding properties of ROR alpha, a novel family of orphan hormone nuclear receptors. Genes & development. 1994; 8:538–553. [PubMed: 7926749]
15. Sun Z, et al. Requirement for RORgamma in thymocyte survival and lymphoid organ development. Science. 2000; 288:2369–2373. [PubMed: 10875923]
16. Deblois G, Giguere V. Oestrogen-related receptors in breast cancer: control of cellular metabolism and beyond. Nature reviews. Cancer. 2013; 13:27–36. [PubMed: 23192231]
17. Flaveny CA, et al. Broad Anti-tumor Activity of a Small Molecule that Selectively Targets the Warburg Effect and Lipogenesis. Cancer cell. 2015; 28:42–56. [PubMed: 26120082]
18. Robinson D, et al. Integrative clinical genomics of advanced prostate cancer. Cell. 2015; 161:1215–1228. [PubMed: 26000489]
19. Solt LA, et al. Identification of a selective RORgamma ligand that suppresses T(H)17 cells and stimulates T regulatory cells. ACS chemical biology. 2012; 7:1515–1519. [PubMed: 22769242]
20. Kumar N, et al. Identification of SR2211: a potent synthetic RORgamma-selective modulator. ACS chemical biology. 2012; 7:672–677. [PubMed: 22292739]
21. Zhang Y, et al. Discovery of 2-oxo-1,2-dihydrobenzo[cd]indole-6-sulfonamide derivatives as new RORgamma inhibitors using virtual screening, synthesis and biological evaluation. European journal of medicinal chemistry. 2014; 78:431–441. [PubMed: 24704616]

22. Xiao S, et al. Small-molecule RORgammat antagonists inhibit T helper 17 cell transcriptional network by divergent mechanisms. Immunity. 2014; 40:477–489. [PubMed: 24745332]
23. Wang Y, et al. Discovery of novel N-(5-(arylcarbonyl)thiazol-2-yl)amides and N-(5-(arylcarbonyl)thiophen-2-yl)amides as potent RORgammat inhibitors. Bioorganic & medicinal chemistry. 2014; 22:692–702. [PubMed: 24388993]
24. Chang MR, Lyda B, Kamenecka TM, Griffin PR. Pharmacologic repression of retinoic acid receptor-related orphan nuclear receptor gamma is therapeutic in the collagen-induced arthritis experimental model. Arthritis Rheumatol. 2014; 66:579–588. [PubMed: 24574218]
25. Kumar N, et al. Identification of SR3335 (ML-176): a synthetic RORalpha selective inverse agonist. ACS chemical biology. 2011; 6:218–222. [PubMed: 21090593]
26. Mendiratta P, et al. Genomic strategy for targeting therapy in castration-resistant prostate cancer. J Clin Oncol. 2009; 27:2022–2029. [PubMed: 19289629]
27. Hu R, et al. Distinct transcriptional programs mediated by the ligand-dependent full-length androgen receptor and its splice variants in castration-resistant prostate cancer. Cancer research. 2012; 72:3457–3462. [PubMed: 22710436]
28. Sharma NL, et al. The androgen receptor induces a distinct transcriptional program in castration-resistant prostate cancer in man. Cancer cell. 2013; 23:35–47. [PubMed: 23260764]
29. Frigo DE, et al. CaM kinase kinase beta-mediated activation of the growth regulatory kinase AMPK is required for androgen-dependent migration of prostate cancer cells. Cancer research. 2011; 71:528–537. [PubMed: 21098087]
30. Zou JX, et al. Androgen-induced coactivator ANCCA mediates specific androgen receptor signaling in prostate cancer. Cancer research. 2009; 69:3339–3346. [PubMed: 19318566]
31. Ciofani M, et al. A validated regulatory network for Th17 cell specification. Cell. 2012; 151:289–303. [PubMed: 23021777]
32. Rene O, et al. Minor Structural Change to Tertiary Sulfonamide RORc Ligands Led to Opposite Mechanisms of Action. ACS medicinal chemistry letters. 2015; 6:276–281. [PubMed: 25815138]
33. Wang Y, et al. Bufalin is a potent small-molecule inhibitor of the steroid receptor coactivators SRC-3 and SRC-1. Cancer research. 2014; 74:1506–1517. [PubMed: 24390736]
34. Asangani IA, et al. Therapeutic targeting of BET bromodomain proteins in castration-resistant prostate cancer. Nature. 2014; 510:278–282. [PubMed: 24759320]
35. Lange T, et al. Aberrant Presentation of HPA-Reactive Carbohydrates Implies Selectin-Independent Metastasis Formation in Human Prostate Cancer. Clinical Cancer Research. 2014; 20:1791–1802. [PubMed: 24526735]
36. Meissburger B, et al. Adipogenesis and insulin sensitivity in obesity are regulated by retinoid-related orphan receptor gamma. EMBO molecular medicine. 2011; 3:637–651. [PubMed: 21853531]
37. Qin J, et al. Androgen deprivation-induced NCoA2 promotes metastatic and castration-resistant prostate cancer. The Journal of clinical investigation. 2014; 124:5013–5026. [PubMed: 25295534]
38. Zhong J, et al. p300 acetyltransferase regulates androgen receptor degradation and PTEN-deficient prostate tumorigenesis. Cancer research. 2014; 74:1870–1880. [PubMed: 24480624]
39. Agoulnik IU, et al. Androgens modulate expression of transcription intermediary factor 2, an androgen receptor coactivator whose expression level correlates with early biochemical recurrence in prostate cancer. Cancer research. 2006; 66:10594–10602. [PubMed: 17079484]
40. Taylor BS, et al. Integrative genomic profiling of human prostate cancer. Cancer cell. 2010; 18:11–22. [PubMed: 20579941]
41. Tien JC, et al. The steroid receptor coactivator-3 is required for the development of castration-resistant prostate cancer. Cancer research. 2013; 73:3997–4008. [PubMed: 23650284]
42. Sharma A, et al. The retinoblastoma tumor suppressor controls androgen signaling and human prostate cancer progression. The Journal of clinical investigation. 2010; 120:4478–4492. [PubMed: 21099110]
43. Li Y, et al. LEF1 in androgen-independent prostate cancer: regulation of androgen receptor expression, prostate cancer growth, and invasion. Cancer research. 2009; 69:3332–3338. [PubMed: 19351848]

44. Zhang L, et al. NF-kappaB regulates androgen receptor expression and prostate cancer growth. The American journal of pathology. 2009; 175:489–499. [PubMed: 19628766]
45. Lee E, et al. Inhibition of androgen receptor and beta-catenin activity in prostate cancer. Proceedings of the National Academy of Sciences of the United States of America. 2013; 110:15710–15715. [PubMed: 24019458]
46. Yu J, et al. An integrated network of androgen receptor, polycomb, and TMPRSS2-ERG gene fusions in prostate cancer progression. Cancer cell. 2010; 17:443–454. [PubMed: 20478527]
47. Antonarakis ES, et al. AR-V7 and resistance to enzalutamide and abiraterone in prostate cancer. The New England journal of medicine. 2014; 371:1028–1038. [PubMed: 25184630]
48. Zhang Q, et al. Interleukin-17 promotes formation and growth of prostate adenocarcinoma in mouse models. Cancer research. 2012; 72:2589–2599. [PubMed: 22461511]
49. Strasner A, Karin M. Immune Infiltration and Prostate Cancer. Frontiers in oncology. 2015; 5:128. [PubMed: 26217583]

References

50. Tsai HC, Boucher DL, Martinez A, Tepper CG, Kung HJ. Modeling truncated AR expression in a natural androgen responsive environment and identification of RHOB as a direct transcriptional target. PloS one. 2012; 7:e49887. [PubMed: 23209612]
51. Yang P, et al. Histone Methyltransferase NSD2/MMSET Mediates Constitutive NF-kappaB Signaling for Cancer Cell Proliferation, Survival, and Tumor Growth via a Feed-Forward Loop. Molecular and cellular biology. 2012; 32:3121–3131. [PubMed: 22645312]
52. Chandran UR, et al. Gene expression profiles of prostate cancer reveal involvement of multiple molecular pathways in the metastatic process. BMC cancer. 2007; 7:64. [PubMed: 17430594]
53. Grasso CS, et al. The mutational landscape of lethal castration-resistant prostate cancer. Nature. 2012; 487:239–243. [PubMed: 22722839]
54. Tamura K, et al. Molecular Features of Hormone-Refractory Prostate Cancer Cells by Genome-Wide Gene Expression Profiles. Cancer research. 2007; 67:5117–5125. [PubMed: 17545589]
55. Ross-Adams H, et al. Integration of copy number and transcriptomics provides risk stratification in prostate cancer: A discovery and validation cohort study. EBioMedicine. 2015; 2:1133–1144. [PubMed: 26501111]
56. Bild AH, et al. Oncogenic pathway signatures in human cancers as a guide to targeted therapies. Nature. 2006; 439:353–357. [PubMed: 16273092]
57. Kalashnikova EV, et al. ANCCA/ATAD2 overexpression identifies breast cancer patients with poor prognosis, acting to drive proliferation and survival of triple-negative cells through control of B-Myb and EZH2. Cancer research. 2010; 70:9402–9412. [PubMed: 20864510]
58. Wei Q, et al. Reduced Expression of Mismatch Repair Genes Measured by Multiplex Reverse Transcription-Polymerase Chain Reaction in Human Gliomas. Cancer research. 1997; 57:1673–1677. [PubMed: 9135006]
59. Li H, Durbin R. Fast and accurate short read alignment with Burrows–Wheeler transform. Bioinformatics. 2009; 25:1754–1760. [PubMed: 19451168]
60. Langmead B, Trapnell C, Pop M, Salzberg SL. Ultrafast and memory-efficient alignment of short DNA sequences to the human genome. Genome biology. 2009; 10:R25–R25. [PubMed: 19261174]
61. Trapnell C, et al. Differential gene and transcript expression analysis of RNA-seq experiments with TopHat and Cufflinks. Nat. Protocols. 2012; 7:562–578. [PubMed: 22383036]
62. Trapnell C, et al. Transcript assembly and quantification by RNA-Seq reveals unannotated transcripts and isoform switching during cell differentiation. Nat Biotech. 2010; 28:511–515.
63. Eisen MB, Spellman PT, Brown PO, Botstein D. Cluster analysis and display of genome-wide expression patterns. Proceedings of the National Academy of Sciences. 1998; 95:14863–14868.
64. Subramanian A, et al. Gene set enrichment analysis: a knowledge-based approach for interpreting genome-wide expression profiles. Proceedings of the National Academy of Sciences of the United States of America. 2005; 102:15545–15550. [PubMed: 16199517]

65. Louie MC, et al. Androgen-induced recruitment of RNA polymerase II to a nuclear receptor-p160 coactivator complex. Proceedings of the National Academy of Sciences of the United States of America. 2003; 100:2226–2230. [PubMed: 12589022]

66. Schmidt D, et al. ChIP-seq: using high-throughput sequencing to discover protein-DNA interactions. Methods. 2009; 48:240–248. [PubMed: 19275939]

67. Langmead B, Salzberg SL. Fast gapped-read alignment with Bowtie 2. Nature methods. 2012; 9:357–359. [PubMed: 22388286]

68. Zhang Y, et al. Model-based analysis of ChIP-Seq (MACS). Genome biology. 2008; 9:R137. [PubMed: 18798982]

69. Nguyen HG, et al. Targeting autophagy overcomes Enzalutamide resistance in castration-resistant prostate cancer cells and improves therapeutic response in a xenograft model. Oncogene. 2014; 33:4521–4530. [PubMed: 24662833]

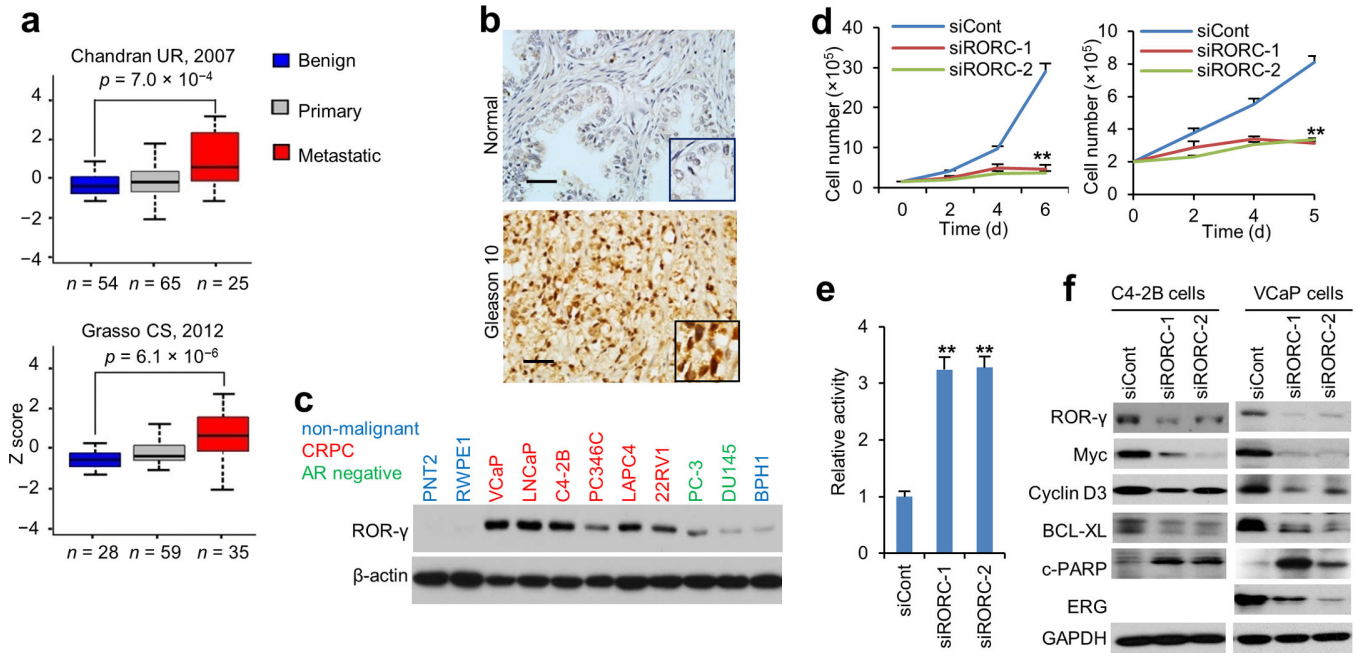

Figure 1. ROR-γ overexpression associates with metastatic CRPC progression and is required for survival of prostate cancer cells

(a) *RORC* transcript levels from two GEO datasets were queried for association with disease status (benign, primary and metastatic). *p* values were calculated using two tail *t*-test. Box plot line (from top to bottom): maximum, Q3, Median, Q1 and minimum, where Q1 and Q3 are the first and third quartile respectively.

(b) Representative images from ROR-γ IHC of normal prostate ($n = 8$) or a cohort of prostate cancer tumor specimens ($n = 70$). Scale bars, 50 μm.

(c) Immunoblotting analysis of ROR-γ protein in prostate cancer and non-cancer cell lines. Shown are representative blot, $n = 4$.

(d) C4-2B (left) in 9% charcoal-dextrand-stripped (cds) FBS plus 1% FBS medium and VCaP (right) in regular FBS medium were transfected with RORC or control siRNA. After indicated times, viable cells were counted. Data shown are mean ± s.d. Student's *t*-test. ** $p < 0.001$, $n = 3$.

(e) C4-2B cells were treated as in (d) and apoptosis was analyzed by measuring caspase3/7 activity. Data shown are mean ± s.d. Student's *t*-test. ** $p < 0.001$, $n = 3$.

(f) Immunobloting analysis of indicated proteins in C4-2B and VCaP cells transfected with RORC or control siRNA and incubated for three days. Shown are representative blot, $n = 3$.

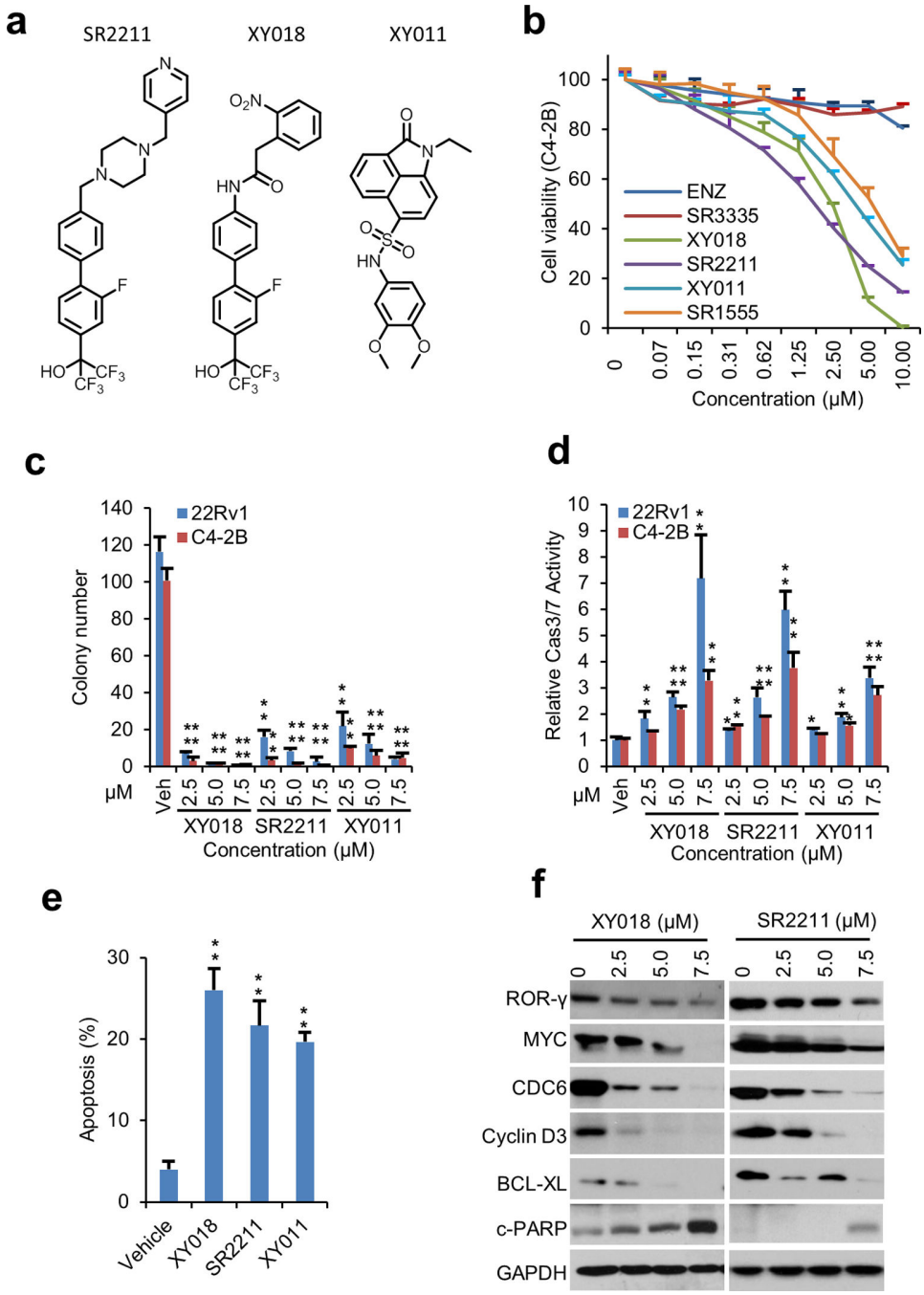

Figure 2. ROR-γ antagonists inhibit growth of CRPC cells

(a) Chemical structures of ROR-γ antagonists SR2211, XY018 and XY011.

(b) Cell viability measured by Cell-Titer GLO of C4-2B cells treated with indicated concentrations of enzalutamide (ENZ), ROR-α agonist SR3335 and ROR-γ antagonists XY018, SR2211, XY011 and SR1555 for 4 days. Experiments were performed with three independent experiments and sextuplicate.

(c) C4-2B and 22Rv1 cells were treated with vehicle or indicated concentrations of SR2211 or XY108 or XY011 for 14 days and colony formation was assessed. * $p < 0.05$, ** $p < 0.01$, $n = 3$.

(d) Caspase-3/7 activities in C4-2B and 22Rv1 cells treated with vehicle or indicated ROR-γ antagonists for 3 days. ** $p < 0.01$, $n = 3$.

(e) TUNEL-positive apoptotic cells treated with vehicle or ROR-γ antagonists (5 μM) were counted and expressed as percentage of total cells. Data shown are mean percentage of apoptotic cells ± s.d. * $p < 0.05$, ** $p < 0.01$, $n = 3$.

(f) Immunoblotting analysis of indicated proteins in C4-2B cells treated with vehicle or indicated ROR-γ antagonists for 3 days. Representative blots, $n = 3$.

All data shown above are mean ± s.d. Significance was calculated using Student's *t*-test.

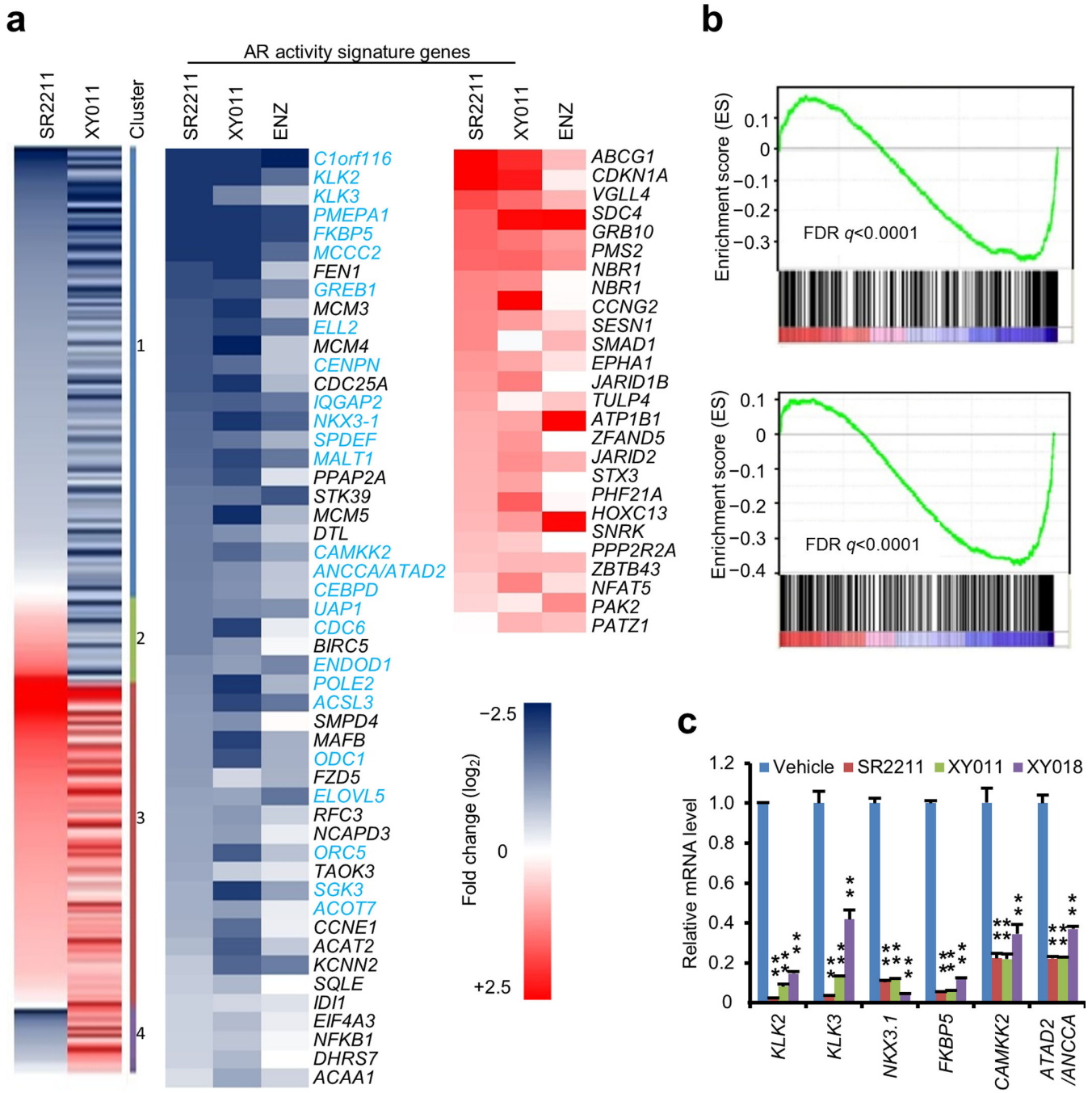

Figure 3. ROR-γ controls AR-dependent gene programs

(a) Heatmap displaying the fold changes of gene expression detected by RNA-seq in C4-2B cells treated with either SR2211 (5 μM), XY011 (5 μM) or ENZ (20 μM) for 48 hours, compared to vehicle. Left, genes that were altered in expression with $\log_2 > 0.5$ in at least one condition are displayed. Cluster 1, genes inhibited by both antagonists; cluster 2, genes induced by SR2211 but inhibited by XY011; cluster 3, genes induced by both antagonists; cluster 4, genes inhibited by SR2211 but induced by XY011. Middle and right, androgen-responsive, AR activity signature genes that were altered in expression are displayed, with

AR target genes in light blue which were defined by AR ChIP-seq peaks, and genes that were also affected by ENZ are also displayed for comparision.

(b) GSEA of the AR activity signature in C4-2B cells treated with 5 μM SR2211 (up) or XY011 (down) compared to vehicle. The signature was defined by genes with significant expression changes by androgen stimulation in PCa cells and androgen deprivation in human tumors[26].

(c) qRT-PCR analysis of indicated genes in C4-2B cells treated with vehicle or ROR-γ antagonists (5 μM) for 48 hours. Data shown are mean ± s.d. Student's *t*-test. ** $p < 0.001$, $n = 3$.

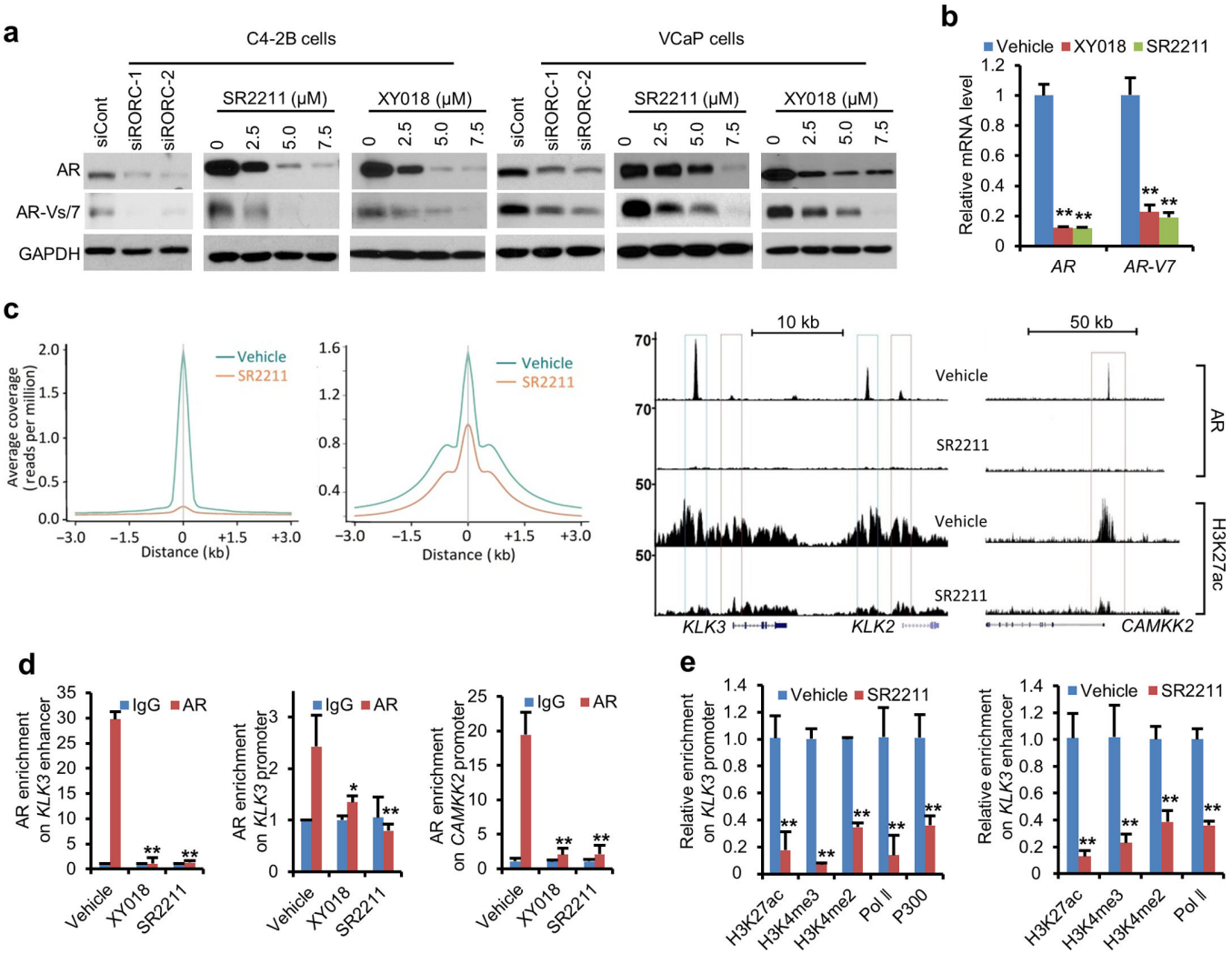

Figure 4. ROR-γ inhibition strongly suppresses AR and its variant expression and eliminates AR genome binding

(a) Immunoblotting of AR (full length) and AR variants in C4-2B or AR-V7 in VCaP cells treated with control or ROR-γ siRNAs, or with ROR-γ antagonists at indicated concentrations for 72 hours. Representative blots, $n = 4$.

(b) qRT-PCR analysis of AR full-length and AR-V7 expression in VCaP cells treated with vehicle, 5 μM XY018 or SR2211 for 48 hours. ** $p < 0.01$, $n = 3$.

(c) ChIP-seq summary plot of AR enrichment (average coverage; left) across AR-binding sites (ARBS) and H3K27ac enrichment (middle) across the indicated genomic distance in different treatments. Right, genome browser display of AR binding and H3K27ac enrichment events on enhancers and/or promoters of AR target genes KLK2, KLK3 and CAMKK2. ChIP-seq was performed in C4-2B cells treated with vehicle or SR2211 (5 μM) for 24 hours.

(d) And (e) ChIP-qPCR analysis of relative AR, p300 and Pol II occupancy, or histone modifications at indicated gene promoter and/or enhancer in C4-2B cells treated with vehicle or 5 μM of XY018 or SR2211 for 24 hours. * $p < 0.05$, ** $p < 0.01$, $n = 3$.

Data shown above are mean ± s.d. Significance was calculated using Student's *t*-test.

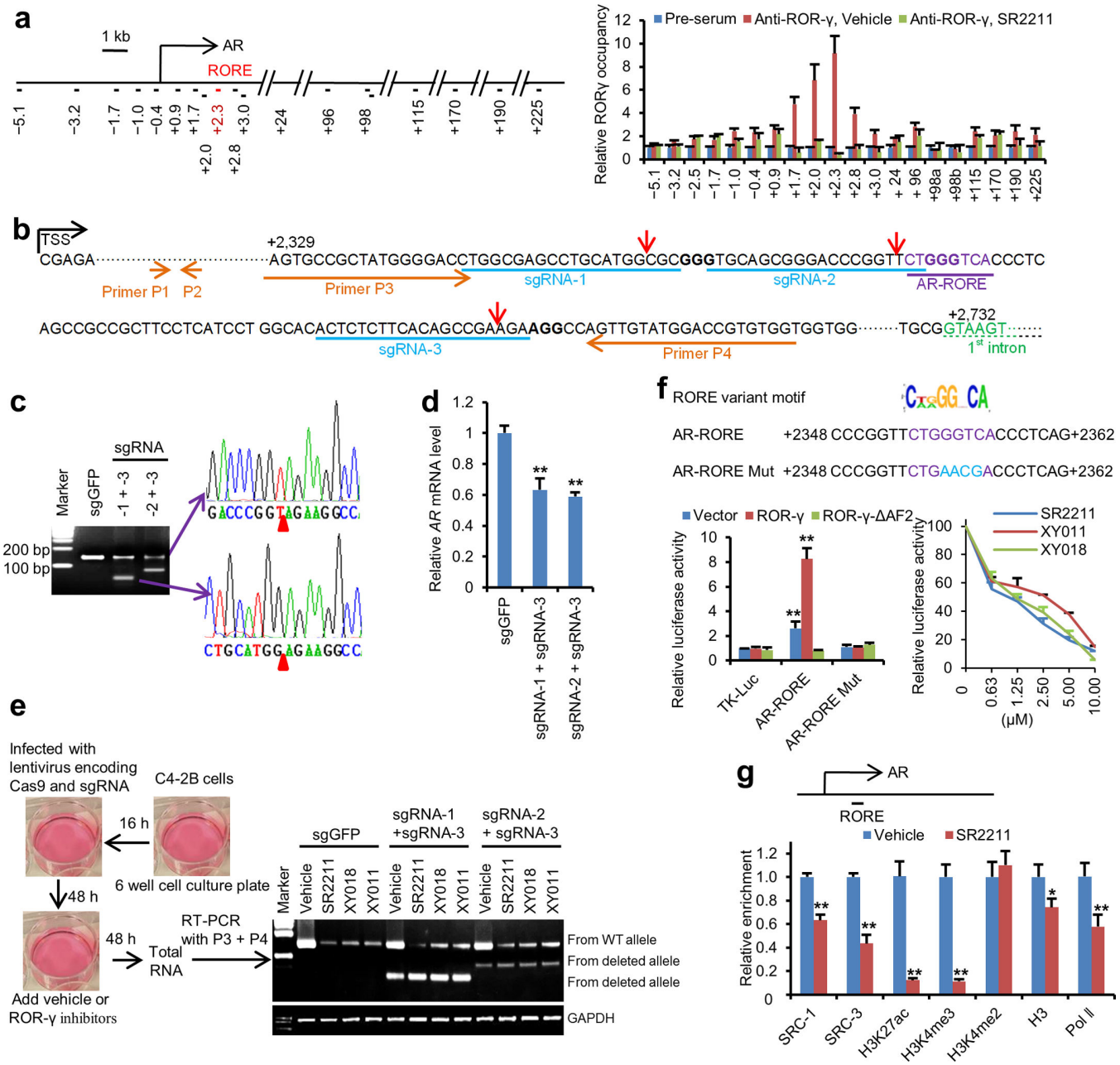

Figure 5. ROR-γ directly controls AR gene expression through an exonic RORE and SRCs

(a) Left, schematics of AR gene locus with ChIP primer-pair locations indicated by horizontal short lines and their distance in kb relative to TSS. The primer pair amplifying the RORE site is in red. Right, ChIP-qPCR analysis of ROR-γ occupancy at the locus in C4-2B cells treated with vehicle or 5μM SR2211. $n = 3$.

(b) Schematic diagram depicting the locations of gRNAs targeting the AR-RORE region, primers used for genomic DNA PCR or RT-PCR and predicted Cas9 cleavage sites (red arrow head). Note: due to the lack of additional PAM sequence at or near the RORE, sgRNA-2 is the only one that can be designed to cause indel type of alterations adjacent to the RORE sequence.

(c) PCR and sequencing analysis of genomic DNA from editing-heterogenous C4-2B cells treated with indicated sgRNAs and Cas9. Genomic DNA PCR was performed using primers p3 and p4. The top band indicates the expected full-length PCR amplicons. The two lower bands indicate the expected PCR amplicons with deletions caused by the indicated sgRNA-guided editing. PCR products containing the deletion amplicons were cloned and sequenced. Representative sequencing chromatograms of expected deletion junctions are shown, $n = 25$). Red arrowheads indicates expected deletion junction.

(d) qRT-PCR analysis with primers p1 and p2 of AR mRNA in C4-2B cells treated with indicated sgRNAs. ** $p < 0.01$, $n = 3$.

(e) Semi-quantitative RT-PCR analysis with primers p3 and p4 of AR mRNA in C4-2B cells treated with indicated sgRNAs and ROR-γ antagonists (5μM, 48 hours), as illustrated at left, for measuring effects of the antagonists on AR mRNA expression from wild type or deleted alleles. Representative gel images are shown, $n = 3$.

(f) Sequences of the wild type (in purple) and mutated (in blue) form of AR-RORE linked to reporters (top). AR-RORE reporter gene assays with 293T cells showing effects of mutating the RORE sequence or ROR-γ (left), or the antagonists (right) on ROR-γ activation. ** $p < 0.01$, $n = 3$.

(g) ChIP-qPCR analysis of relative occupancy by indicated proteins at the AR-RORE site in C4-2B cells treated with vehicle or 5μM SR2211 for 24 hours. * $p < 0.05$, ** $p < 0.01$, $n = 3$. Data shown are mean ± s.d. Significance was calculated using Student's *t*-test.

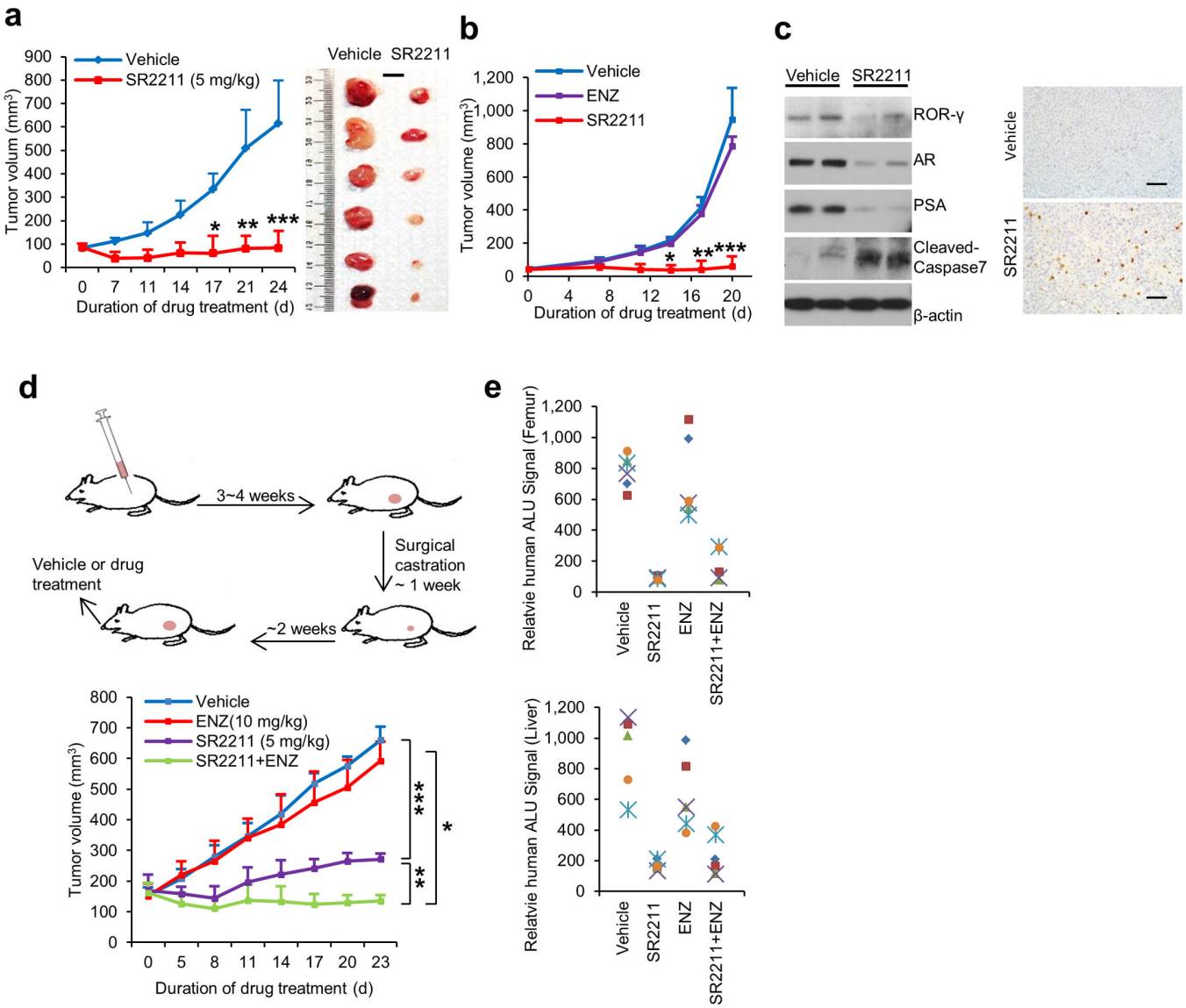

Figure 6. ROR-γ antagonists potently inhibit tumor growth and metastasis

(a) and (b) Effects of indicated treatments (SR2211, 5 mg/kg, i.p., 5 times a week; ENZ, 10 mg/kg, oral, 5 times a week; or vehicle) on growth of C4-2B or 22Rv1 xenografts ($n = 6$ mice per group). Treatment started when C4-2B tumors reached approximately100 mm^3, or 22Rv1 tumors reached approximately 50 mm^3. Mean tumor volume ± s.e.m and representative tumor images are shown. Scale bar is 1cm. Significance was calculated using Student's *t*-test with the following *p* values: for C4-2B exnografts, * $p = 0.000293$, ** $p = 6.67E-05$, *** $p=1.13E-05$; for 22Rv1 xenografts, # $p = 3.03E-08$, ** $p = 1.77E-09$, *** $p = 1.14E-08$.

(c) Immunoblotting (left) of C4-2B xenograft tumors after 24 days of treatment with vehicle or SR2211 as in (a). Cell lysate for each lane was from homogenized tumor tissues randomly combined from three mice of vehicle or SR2211 group. Anti-cleaved caspase-3 IHC images of tumor sections were shown at right. Scale bar is 50 μm.

(d) Schematics illustrating CRPC-VCaP xenograft tumor establishment and treatment (left). Castrated mice bearing the CRPC-VCaP xenografts (n = 6 mice per group) received vehicle, SR2211 (i.p.; 5 mg/kg), ENZ (oral; 10 mg/kg), or a combination of SR2211 and ENZ, as indicated, 5 times a week. Mean tumor volume ± s.e.m was shown. Significance was calculated using Student's t-test. * p = 1.98E-10, ** p = 1.46E-10, *** p = 7.21E-13.
(e) Mice bearing VCaP xenografts as in (d) treated with vehicle, SR2211, ENZ or combination for 23 days were assessed for spontaneous metastasis to the femur (bone marrow) and liver. Genomic DNA isolated from these sites was analyzed for metastasized cells by measuring human Alu sequence (by Alu-qPCR).